Intense rift magmatism caused rapid thickening of Yilgarn Craton crust at 2.7 Ga

Alan R.A. Aitken [*], Q. Masurel, N. Thébaud, Lu Li [iD], Abdul Azim bin Rossalim [iD]

Centre for Exploration Targeting, School of Earth Sciences, The University of Western Australia, Perth, Western Australia, Australia

ARTICLE INFO

ABSTRACT

The crustal structure of many Archean cratons fits a paradigm of relatively thin crust (< 35 km), with felsic compositions, low-velocity lower crust and a sharp Moho discontinuity. This contrasts with the crusts of Proterozoic regions, which are typified by thicker crust (> 40 km), often with a high-velocity lower crust and a diffuse Moho. A global-scale transition in the nature of the crust is suggested, but its timing and nature remain unclear. The Yilgarn Craton in Western Australia has crustal thickness from ~ 30 km to > 45 km and may preserve a key example of this transition. This study employs seismic-constrained gravity inversion to resolve in detail the thickness and density of the Yilgarn Craton crust. Regions with thick and dense crust are identified, and we explore two scenarios for their development: scenario 1 involves crustal shortening, erosion, and the development of a garnet-bearing lower crust, and scenario 2 involves addition of mafic magmatic rocks during extension. Scenario 2 is more consistent with the Neoarchean geology of the craton and the inferred extents of juvenile magmatism between 2.73 to 2.65 Ga. A regional stratigraphic unconformity at ca. 2.73 Ga is recognised as a turning point in the evolution of the craton, marking the crossing of thermo-rheological thresholds for geodynamically-stable lower crust. We suggest that net crustal thickening occurred over the next $\sim$40 Ma with a mafic magmatic input totalling 5.0 Mkm^3 balanced by moderate extension (β-factor ~ 1.1) Monte-Carlo simulations use a time-and-space distributed series of events of <40 Ma duration and <10 MKm^3 vol to successfully explain modelled variations in global average crustal thickness through time. The event identified here aligns with a peak in constructive tendency, supporting the diachronous and episodic growth of the global lower crust during the Neoarchean.

1. Introduction

How the thickness and composition of the Earth's crust have evolved through time remains a contentious issue (Dhuime et al., 2015; Hawkesworth et al., 2020; Keller and Harrison, 2020; Korenaga, 2018). Global-scale analyses of present-day crustal thickness reveal only weak relationships of crustal thickness and properties with province ages (Mooney et al., 2023; Szwillus et al., 2019). The ability of these global-scale analyses to resolve key events and processes is, however, limited by the coarse-scale averaging of data in both time and space, and the lack of clear knowledge of the timing of formation of the lower-crust relative to the upper-crust.

More detailed spatial analysis of the crusts of Archean cratons, as preserved today, suggests a distinct 'Archean' paradigm for crustal structure. This paradigm involves a thin crust (<35 km) with low density combined with low seismic velocity in the lower crust and a sharp and flat-lying Moho. This structure is predominant in Mesoarchean cratons, but declines in frequency in Neoarchean cratons and is not found in younger crusts (Abbott et al., 2013). The Proterozoic Eon is typified by relatively thick (> 40 km) and high-density crust with a more gradational Moho (e.g. Abbott et al., 2013). This points to a significant, but poorly characterised change in global crust-forming processes during the Neoarchean.

From geochemical evidence, the dominant process of Archean crust formation was the melting of a garnet-bearing mafic lower crust (Moyen and Martin, 2012). Such lower crust, while potentially thick (Brenhin Keller and Schoene, 2012), is thought to have unstable and removed by processes such as delamination (Johnson et al., 2014). The development of long-term thick crust has been related to the onset of geodynamic stability for garnet-bearing lower crusts (Abbott et al., 2013; Johnson et al., 2014; Mai and Korenaga, 2022; Tang et al., 2020; Yuan, 2015). Stability is primarily driven by mantle potential temperature, that peaks

---

before or during the Neoarchean, and reduces relatively slowly, but not necessarily smoothly (Ganne and Feng, 2017; Herzberg et al., 2010). As thermal thresholds in mantle circulation (Tang et al., 2020), crustal rheology (Mai and Korenaga, 2022) and mineralogy (Johnson et al., 2014) are crossed, the lower crust may stabilise fairly rapidly.

To define how thick crusts have formed during and since the Neoarchean, a detailed understanding is needed of crust-forming processes and their timescales in specific regions, and how these may accumulate to drive the global-scale evolution of crustal thickness. The Yilgarn Craton (hereafter – the craton) in Western Australia is an established testbed for Archean crustal growth hypotheses. The craton has extensive and well-understood late Mesoarchean to Neoarchean geology (Masurel et al., 2022; Masurel and Thébaud, 2024) a well-resolved isotopic record of Archean crustal growth (Mole et al., 2019; Schreefel et al., 2024; Smithies et al., 2024), and minimal post-Archean reworking (Goscombe et al., 2019). Most critically, the craton has highly variable structure, with good geophysical definition, that suggest a secular evolution of the crust (Yuan, 2015).

This study applies a seismic-constrained gravity inversion ensemble to define the thickness and density of the craton's crust. Using these results, two scenarios are tested for the development of the present-day crust from a Mesoarchean Yilgarn proto-craton with crustal structure conforming to the 'Archean' paradigm. The first scenario considers crustal thickening due to shortening, and densification through lower-crust garnet formation and erosive removal of the upper crust. The second scenario considers crustal thickening and densification due to the addition of mafic material to the lower-middle crust. Considering isotopic and geological data, we interpret that crustal thickening occurred in the period 2.73 to 2.69 Ga predominantly due to magmatic addition under moderate extension (β-factor ~1.1). The mechanism of this rapid transition in crustal structure and its timing are discussed with relevance to understanding global crustal-structure evolution.

2. The Yilgarn Craton crust

The crust of the Yilgarn Craton has been mapped with a range of geophysical techniques, giving a comprehensive knowledge of the Moho (Fig. 1), most-recently summarised in Kennett et al. (2023). The thinnest crust is approximately 30 km thick, but extensive areas exceed 40 km thickness and localised areas reach 50 km thickness (Kennett et al., 2023). In receiver function studies, the Moho is generally sharp but several areas of the craton have a gradational Moho signature (Reading
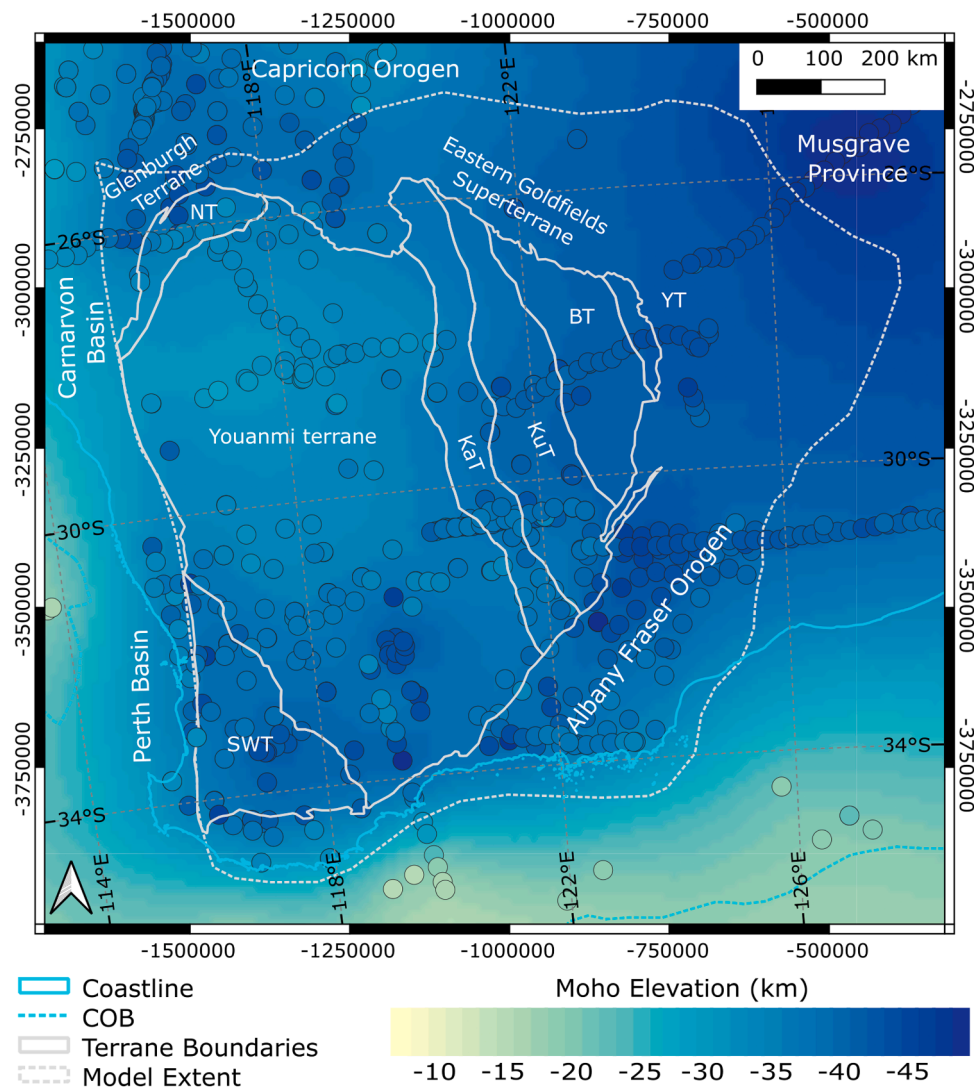

Fig. 1. Moho elevation, showing point values from Kennett et al. (2023) and the kriged surface used as input to the gravity inversion. See supplement for the details of the kriging. The tectonic architecture of the craton is indicated with the terranes of the craton and its outline at the surface demarcated in solid light grey (after Cassidy et al. 2006). The model extent demarcated in dashed light grey covers the exposed craton, its reworked margins and extension of the craton under basins. NT – Narryer Terrane, SWT – Southwest Terrane, KaT – Kalgoorlie Terrane, KuT – Kurnalpi Terrane, BT – Burtville Terrane, YT – Yamarna Terrane.

et al., 2007). Yuan (2015) define in Western Australia an increase in crustal thickness from ~28 km to ~42 km for crust initially formed from 3.4 to 2.8 Ga, with accompanying variations in bulk Vp/Vs, interpreted to reflect secular crust evolution. Variations in crustal thickness and properties are, to a large degree, consistent with the major tectonic subdivisions of the craton.

The Youanmi Terrane crust formed from ca. 3.10 to 2.65 Ga (Mole et al., 2019) and is thinner than elsewhere in the craton. Reflection seismic studies in the northern Youanmi Terrane indicate a two-layer crust with a low-reflectivity upper crust overlying a high reflectivity lower crust and a sharp and flat-lying Moho (Calvert and Doublier, 2018). In the same region, receiver function studies indicate a low crustal Vp, variable Vp/Vs and a sharp Moho discontinuity (Yuan, 2015). Recent isotopic studies have identified two regions of anomalous juvenile magmatism; in the Cue isotopic zone (ca. 2.82 to 2.76 Ga), and in the southern isotopic zone (Smithies et al., 2024). The Cue isotopic zone is not distinguished in the geophysical properties of the crust, however, the southern isotopic zone has thicker crust (Fig. 1).

The Narryer Terrane has the oldest crust of the Yilgarn Craton, aged 3.730 to 2.995 Ga (Mole et al., 2019), and has thicker crust with a double Moho. In receiver function studies, the upper Moho is sharp while the lower Moho has low contrast (Reading et al., 2007). The Narryer Terrane has a complexly deformed structure representing overthrusting of the Narryer Terrane onto the Youanmi Terrane and underthrusting of the Glenburgh Terrane beneath the Narryer Terrane (Sellars et al., 2022).

The South West Terrane is separated from the Youanmi Terrane by the Corrigin Tectonic Zone (Quentin De Gromard et al., 2021). The South West Terrane experienced major crust-forming events in the period ca. 2.710 to 2.665 Ga, and an older evolution extending back to ca. 3.420 Ga. This region is defined in receiver functions by a thicker crust than the Youanmi Terrane, with higher Vp and high Vp/Vs ratio (Yuan, 2015).

The Eastern Goldfields Superterrane (EGST) preserves a younger crust than the Youanmi Terrane and may be subdivided into several terranes, from west to east, the Kalgoorlie, Kurnalpi, Burtville, and Yamarna terranes (Fig. 1). The Kalgoorlie and Kurnalpi terranes preserve juvenile crust formed between ca. 2.73 to 2.69 Ga (Masurel et al., 2022). Large-scale seismic reflection lines across the EGST resolve an eastwards-thickening two-layer crust defined by major flat-lying structures (Calvert and Doublier, 2018). The Moho becomes less distinct as the crust thickens. Receiver functions from the EGST define a thick crust with high Vp, but a low Vp/Vs ratio (Yuan, 2015) indicating a more mafic composition.

The north, northeast and southeast margins of the craton were reworked during the Proterozoic. In the Capricorn and Albany Fraser orogens, the craton margin is overlain by Paleoproterozoic basins (Occhipinti et al., 2017; Spaggiari et al., 2015), and is partly rifted (Glasson et al., 2019; Ramos et al., 2021). In each, widespread deformation occurred during Paleoproterozoic orogenesis (Occhipinti et al., 2017; Spaggiari et al., 2015). In the Albany Fraser Orogen, basin formation and orogenesis continued into the Mesoproterozoic (Spaggiari et al., 2015). To the northeast the craton has been interpreted to extend beneath the Officer Basin to a fault contact with the Mesoproterozoic crust of the Musgrave Province (Korsch and Doublier, 2016). The Phanerozoic Perth and Carnarvon basins bound the craton to the west and overlie the Pinjarra Orogen (Markwitz et al., 2017).

The lithospheric mantle of the craton is also variable in its nature. The lithosphere thickness, excluding areas in the west and south affected by the rifting of Gondwana, is fairly consistent at ~200 km and furthermore, the lower lithosphere has fairly homogenous seismic velocity (Kennett et al., 2013). Contrastingly, the upper lithospheric mantle has a distinct contrast in seismic velocity between the Youanmi Terrane and the EGST (Kennett et al., 2013). The high-velocity mantle under the Youanmi Terrane, with a highly Fe-depleted composition (Tesauro et al., 2020) has been interpreted as the original Archean

cratonic mantle, dating to cratonisation at ~2.82 Ga (Mole et al., 2019). In contrast, the mantle under the EGST is significantly more Fe-fertile (Tesauro et al., 2020) which has been linked to Proterozoic magmatic refertilisation events (Aitken et al., 2023).

3. Methods

3.1. Gravity inversion

The gravity inversion approach followed several prior studies (Aitken, 2010; Aitken et al., 2013a; Alghamdi et al., 2018; Li and Aitken, 2024; Moro et al., 2023). A seven-layer initial model was generated from compilations of crustal interfaces, including the topographic surface (Whiteway, 2009), the base of Phanerozoic (Geognostics Australia Pty Ltd, 2021) and Proterozoic (de Vries et al., 2008) sedimentary basins, and the Moho (Kennett et al., 2023). Greenstone belts and mafic intrusions are prominent features of the gravity field. To represent these, an 'upper crust mafic' layer was derived from high-pass filtered gravity data as an equivalent thickness layer using a density of 2850 kg/m^3. The details of the initial model construction are described in the supplementary material. Free-air gravity data were extracted from the national gravity grid (Lane et al., 2020), upward continued by 5 km, and a long-wavelength trend was removed using degree/order 15 and below from the Eigen6C4 gravity model (Foerste et al., 2014).

Prior to inversion the initial density model was optimised to correct for inaccuracies in the definition of density within the deep crust and mantle, which dictate the density contrast at the Moho, which was the dominant feature of the residual gravity field. An optimal fit to the gravity data was found with a crustal density law of $2670 + 0.013{*}z$ kgm^{-3}, and a mantle density law of $3270 + 0.0002{*}z$ kgm^{-3}, with z depth in km.

An iterative approach was used with 20 cycles of alternating inversions solving for boundary depths (geometric inversion) and density values (density inversion). The relative importance of geometry vs density inversion is controlled by per-iteration constraints. These were varied to generate an ensemble result that captures the impact of this ambiguity (Aitken et al., 2013a). Bias indicates the degree to which misfit was resolved through density inversion (positive bias) or geometry inversion (negative bias) (Alghamdi et al., 2018). High bias indicates instability, and results with bias > 1 or < -1 were rejected. Model results with more than 15 % misfit remaining relative to the initial misfit were rejected. The mean RMS misfit for the ensemble of accepted results was 3.8 mGal, approximately the gravity effect of a Moho deviation of 225 m.

The inversion results were verified with posterior constraints (Moro et al., 2023) from AuSeis seismic analyses, which resolve crustal thickness and density from P-wave coda (Qashqai and Saygin, 2019). For each ensemble member, we assess the fit through a misfit score defined as RMS of the interquartile distances from the median AuSeis outcomes. In this case, all ensemble results were within the range of AuSeis constraints and showed a similar overall fit, but with variable fit to density and thickness (Fig. 2).

3.2. Crust reconstruction

Models of crustal evolution in the craton indicate para-autochthonous geological development during the Neoarchean by rifting of a Mesoarchean proto-craton represented today by the Youanmi and Burtville terranes (Masurel et al., 2022; Mole et al., 2019; Pawley et al., 2012; Smithies et al., 2024). We sought to reconstruct the crust to a reference crust representing this proto-craton. As reference crust, we selected properties for the thinnest crust in the central Youanmi Terrane, with a thickness $H_{Reference}$ of 30 km and a crustal density $\rho_{Reference}$ of 2800 kg/m^3. The reconstruction involved two steps.

Step 1: Remove basins and mafic rocks
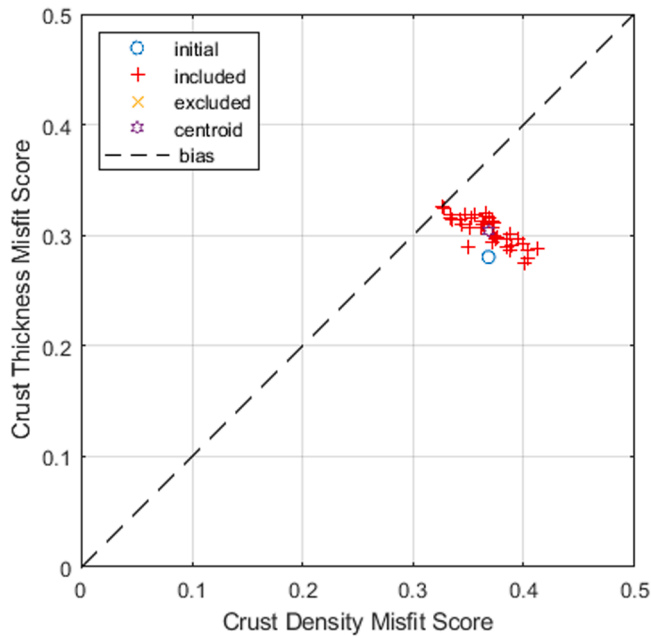The loads of the Phanerozoic and Proterozoic sedimentary basin

Fig. 2. Inversion ensemble results compared to AuSeis. A misfit score of < 0.25 is within the interquartile range of AuSeis results, while values exceeding 0.5 are outside the range of AuSeis results. Ensemble member weights are assigned according to the distance from the origin. For this ensemble no results were excluded based on their fit to AuSeis.

layers were removed considering that deposition involved grains settling into seawater within a topographic depression, which in turn had displaced a felsic upper crust. The excess mass for each basin layer was calculated as:

$$M_{Sed} = t_{Basin} \times (\rho_{Basin} - \rho_{Felsic}),$$

where t_{Basin} and ρ_{Basin} were the thickness and density of the basin layer from the inversion model results and ρ_{Felsic} was 2690 kgm^{-3}, the mean density of felsic gneisses at amphibolite facies (Rudnick and Fountain, 1995). The loads of mafic rocks in the upper crust were removed considering that they were either intruded into the felsic crust, or erupted as lavas into topographic depressions in the felsic crust. Their excess mass was defined as.

$$M_{Mafic} = t_{Mafic} \times (\rho_{Mafic} - \rho_{Felsic})$$

where t_{Mafic} and ρ_{Mafic} were the thickness and density of the upper crust mafic layer from the inversion model results. Conserving total crust thickness, H, the required adjustment to crystalline crust thickness was calculated as

$\Delta t_{Cryst} = t_{Basin1} + t_{Basin2} + t_{Mafic}$ and the revised density of the crystalline crust was defined as

$$\rho_{Cryst} = (t_{Cryst} \times \rho_{Cryst} + \Delta t_{Cryst} \times \rho_{Felsic})/(t_{Cryst} + \Delta t_{Cryst})$$

Where t_{Cryst} was the thickness of the crystalline crust in the inversion result.

Step 2: Reconstruct the reference crust

Following step 1, two factors remain – the thickness and density of the crystalline crust. For this step, two contrasting scenarios were tested to reconcile the crustal density to the reference state, and then to derive the residual thickness of the reference crust. The residual thickness was used to define the shortening or extension required to achieve present-day thickness. This is expressed as a whole crust stretching factor β representing the proportional bulk crustal strain, being > 1 for net extension and < 1 for net shortening. The first scenario is that the crust was thickened by shortening and structural thickening, with a density

increase due to erosion of the felsic upper crust and the addition of garnet to the lower crust. The second scenario is that the crust was thickened by additions of large volumes of mafic magma to the crust.

Scenario 1 – Crustal thickening through horizontal shortening

Excess crustal thickness was established as $\Delta H = H - H_{Reference}$. Density values in Rudnick and Fountain (1995) define, for a mafic lower crust, that average garnet-bearing mafic granulites are 96 kg/m^3 more dense than average non-garnet bearing granulites; for an anorthositic lower crust the difference is 150 kg/m^3. In each case, this corresponds to the addition of 16–17 % garnet at a density, ρ_{Garnet}, of 3600 kg/m^3. Therefore, we considered that excess thickness, where it caused H to exceed 30 km (~0.8 GPa), involved the addition of a mass of garnet at a specified concentration, C_{Garnet}, in this case 0.16.

$M_{Garnet} = (\rho_{Garnet} - \rho_{Cryst}) \times \Delta H \times C_{Garnet}$

The de-garnetised crustal density was calculated as

$\rho = (H \times \rho_{Cryst} - M_{Garnet})/H$

The remaining excess density was explained through the removal of a felsic upper crust by erosion. To recover the reference density the amount of erosion required was calculated as $\Delta H_{Erod} = H \times (\rho - \rho_{Reference})/(\rho_{Reference} - \rho_{Felsic})$ and the former crustal thickness, including the eroded material, was recalculated as $H_0 = H + \Delta H_{Erod}$ From this, we calculated the required 'extension' expressed as β-factor.

$\beta = H_0/H_{Reference}$

Scenario 2 – Crustal thickening through magmatic addition

Mafic-ultramafic magmatic additions, for example through underplating or sill intrusions, contribute both thickness and density to the crust. This process is likely to be offset by crustal extension, and so we sought to fit the crustal density and leave crustal thickness as the variable to define.

First, we calculated the mass removal (or addition) needed to reach the reference crustal density

$\Delta M_{crust} = H \times (\rho_{Cryst} - \rho_{Reference})$ and for this mass a corresponding thickness of mafic material is calculated as

$\Delta H_{mafic} = \Delta M_{crust}/(\rho_{Mafic} - \rho_{Reference})$

Where ρ_{Mafic} is the density of added material. We used the mean density of mafic granulites at 3038 kg/m^3 (Rudnick and Fountain, 1995). Then we calculated the residual thickness of pre-existing crust, as $H_0 = H - \Delta H_{mafic}$. From this, we then calculate the required extension expressed as β-factor.

4. Results

4.1. Inversion results

The inversion results revealed the crustal structure of the craton in finer detail and shows a distinct region of 30–35 km thick crust in the northern Youanmi Terrane, including the Cue isotopic zone, and thicker crust in the southern Youanmi Terrane and Southwest Terrane, reaching 40 km. The northern edge of the Youanmi Terrane and the Narryer Terrane sit above a gradient to thick crust in the Capricorn Orogen. The EGST shows sytematically thicker crust, 40–43 km, the boundary of which approximately follows the Ida Fault that defines the upper-crustal boundary between the Youanmi Terrane and EGST (Fig. 3). The Corrigin Tectonic Zone, interpreted as the boundary between the Youanmi and South West terranes, is not a marked boundary in the crustal thickness. The Albany Fraser Orogen margin has a distinctly thick crust, while to the northeast, the crust thickens markedly toward the Musgrave Province, reaching over 45 km thick (Fig. 3).

Crustal density shows a distinct co-variation with crustal thickness, with, in general, thicker crust being denser. Key features include the low-density crust of the northern Youanmi Terrane (2800 to 2850 kg/m^3) and Narryer Terrane contrasting with higher-density crust in the southern Youanmi Terrane and Southwest Terrane (2850 to 2875 kg/m^3). The EGST shows an increase in density relative to the Youanmi Terrane. A further increase to densities > 2875 kg/m^3 is seen in the southern Kurnalpi Terrane, Burtville Terrane and Yamarna Terrane.
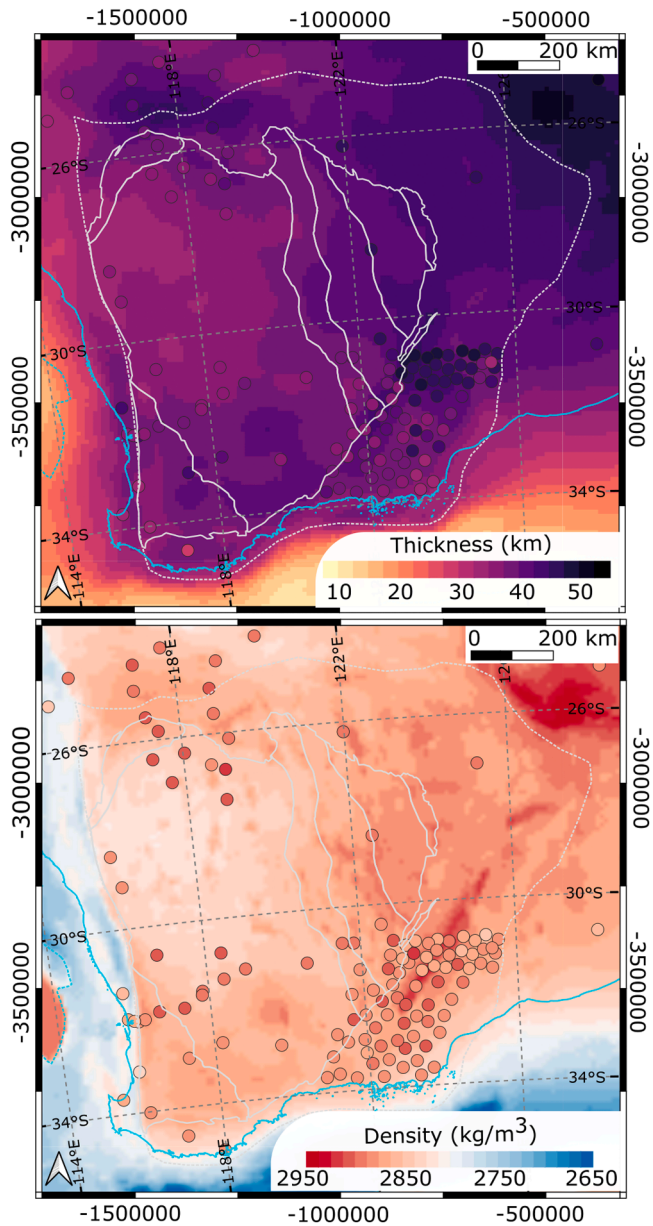
Fig. 3. Mean crustal thickness (a) and mean crustal density (b) from the inversion ensemble, with median crustal thickness and crust density from AuSeis seismic analyses overlaid. The crustal density here includes basins and upper crust mafic rocks.

Crustal densities > 2900 kg/m^3 are found in the Fraser Zone of the Albany Fraser Orogen and in the Musgrave Province, while densities < 2800 kg/m^3 are found in the basin regions to the west and south.

4.2. Crustal reconstruction scenario 1

The first reconstruction scenario investigated the growth of a thick and dense crust through bulk crustal shortening and structural thickening. The objective was to achieve the reference crustal density by removing the effects of the growth of garnet in the lower crust and the erosive removal of the felsic upper crust. The results are tectonically plausible with a total residual crustal thickness of up to 70 km (Fig. 4a), including differential erosion of up to 25 km (Fig. 4b). The implication is that thickening over time was offset by erosion. Reconstructing the residual crustal thickness volume to the reference thickness yields β-factor of 0.3 to 1 (Fig. 4c).
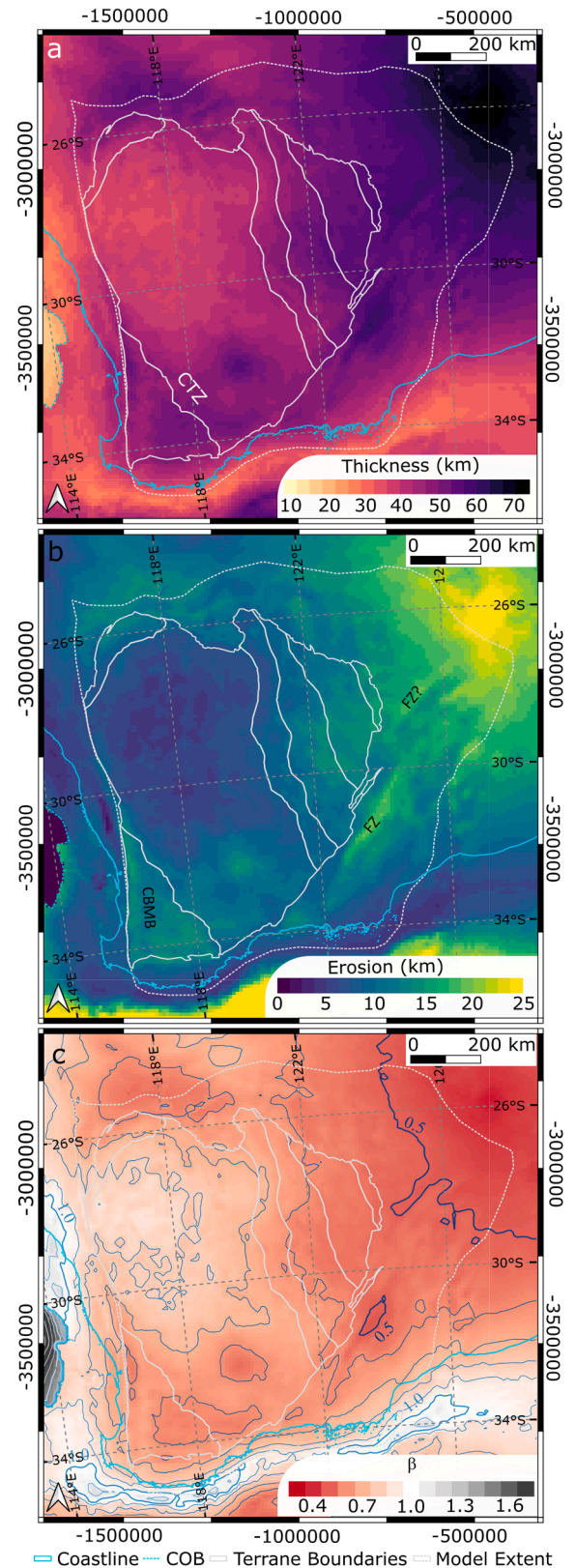

Fig. 4. Crustal reconstruction scenario 1 showing a) residual crustal thickness after the reconstruction process was applied b) erosion relative to reference crust c) β-factor relative to reference crust. CTZ – Corrigin Tectonic Zone, FZ – Fraser Zone, FZ? – possible Fraser Zone equivalent, CBMB – Chittering-Balingup Metamorphic Belt. The reference crust has thickness of 30 km, and density of 2800 kg/m^3.

This reconstruction yields β-factor < 0.8 in the EGST, the South West Terrane and the southern Youanmi Terrane, while the northern Youanmi Terrane and Narryer Terrane have β-factor > 0.8. β-factor reaches a minimum of 0.53 within the limits of the exposed craton. β-factor is < 0.65 in the Capricorn and Albany Fraser orogens, and local minima occur in the Fraser Zone of the Albany Fraser Orogen (0.48), and adjacent to the Musgrave Province (0.43).

This reconstruction scenario demands that, relative to the Youanmi Terrane, the EGST and South West Terrane were shortened by as much as 1.5 times, and in the process, experienced erosive removal of up to 20 km of upper crust. The Proterozoic margins of the craton are shortened by at least 1.5 times, and up to 2 times, including erosive removal of up to 25 km of upper crust. The geological support for this reconstruction scenario is considered in the discussion, considering sedimentary, metamorphic and structural constraints.

4.3. Crustal reconstruction scenario 2

The second crustal reconstruction scenario investigated the growth of a thick and dense crust through magmatic addition. The objective was to achieve the reference crustal density through mafic magmatic addition. The results are tectonically plausible with a residual crustal thickness of 23 to 34 km, magmatic additions of up to 23 km thickness and β-factor between 0.8 and 1.4. Within the exposed craton, β-factor is typically below 1 in the northern Youanmi Terrane, reaching a minimum of 0.89. Maximum β-factor in the exposed craton is 1.17 in the western edge of the South West Terrane, but more broadly is between 1.0 and 1.1 in the EGST, South West Terrane and southern Youanmi Terrane. Residual crustal thickness, magmatic addition and β-factor are variable in the Proterozoic orogens: β-factor is generally above 0.9 and below 1.1, except locally higher values in the Bryah Rift and Earaheedy Basin and in the Fraser Zone of the Albany Fraser Zone, where it reaches 1.25. Towards the northeast, β-factor increases beneath the Officer Basin, reaching ~1.4 at the margin with the Musgrave Province.

This reconstruction scenario suggests that while much of the craton may have been extended, the net extension is moderate, with β-factor of ~ 1.1. However, it is accompanied by an intense magmatic addition to the lower crust of approximately 8 to 15 km of mafic material, comprising a total addition of 5.0 MKm³. For comparison, the Cretaceous High-Arctic Large Igneous Province has a geophysically-defined crustal addition of ~ 20 MKm³ comprising 6 MKm³ in the upper crust and over 13 MKm³ in the lower crust (Oakey and Saltus, 2016).

5. Discussion

5.1. Shortening of the craton margins

We highlight regions where metamorphic and structural events indicate extensive tectonic shortening occurring during the late Neoarchean and into the Proterozoic. As well as the Capricorn and Albany Fraser orogens, these tectonically affected zones include the Narryer Terrane (Sellars et al., 2022; Tucker et al., 2024) and the western edge of the South West Terrane — Chittering and Balingup metamorphic belts (Quentin De Gromard et al., 2021). In these regions the scenario 1 reconstruction is preferred with shortening as the major cause of crustal thickening, and differential erosion of 10–13 km and a β-factor of 0.5 to 0.7.

The Fraser Zone of the Albany Fraser Orogen preserves a thick mafic intrusive complex emplaced into the crust at ca. 1.30 Ga, and a similar crustal feature is found along strike beneath the Officer Basin (Fig. 5). One interpretation of the tectonic setting of this complex is a back-arc rift (Glasson et al., 2019). Our analysis in scenario 2 indicates a residual crust thickness of 25–26 km, with 14–19 km of mafic input required and β-factor of 1.1 to 1.2. A compressional setting has also been suggested, and scenario 1 would indicate differential erosion of 15 km, and a β-factor of 0.5 to 0.6.
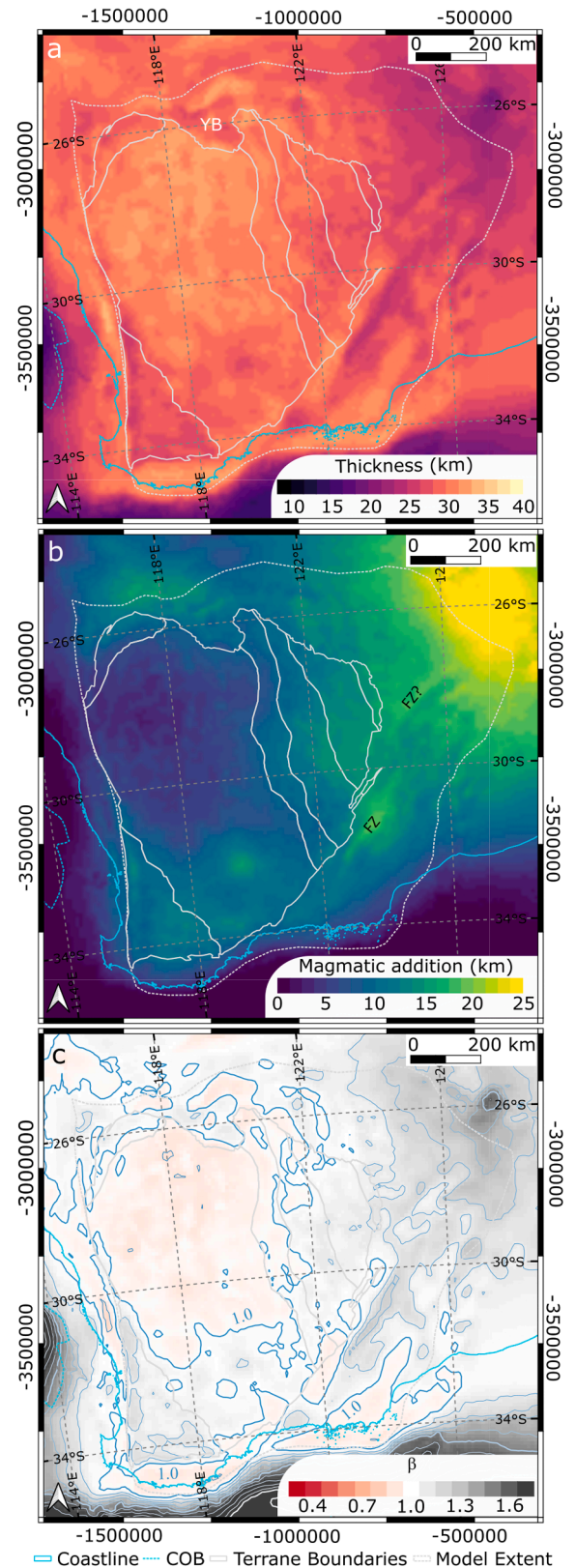

Fig. 5. Crustal reconstruction scenario 2 showing a) residual crustal thickness after the reconstruction process was applied b) differential magmatic input relative to reference crust c) differential β-factor relative to reference crust. YB – Yerrida Basin, including the Bryah Sub-basin, FZ – Fraser Zone, FZ? – possible Fraser Zone equivalent. The reference crust has thickness of 30 km, and density of 2800 kg/m³.

5.2. Proterozoic rifting effects

Several areas have experienced Proterozoic rifting, causing basin development and mafic magmatism, and the interpreted refertilization of the lithospheric mantle (Aitken et al., 2023). The Yerrida Basin in the northern Yilgarn Craton formed between 2.2 and 1.8 Ga with an early phase dominated by crustal sag and magmatic input with relatively little extension (Occhipinti et al., 2017), proceeding to localised rifting in the Bryah Rift (Ramos et al., 2021), where extension is greatest (Fig. 5). Outside the Bryah Rift, the Archean upper crust continues beneath the Yerrida Basin without deformation (Occhipinti et al., 2017) suggesting that only the lower-middle crust was extended. In scenario 2, this region is characterised by a thinned relict Archean crust (~25 km), mafic magmatic addition of 8 to 10 km, locally 13 km in the Bryah Rift, and a β-factor of 1.0 to 1.1. The contemporaneous Earaheedy Basin lacks magmatic rocks in the basin sequence but shows β-factor of 1.0 to 1.1, similarly interpreted to represent thinning of the middle to lower crust. To the northeast, the Yilgarn Craton has been considered to extend to the Musgrave Province (Korsch and Doublier, 2016). Here we see in scenario 2 a distinct gradient of residual crust thickness reducing to the northeast, reaching a minimum of 24 km. Corresponding increases in magmatic addition, exceeding 20 km, and β-factor of up to 1.4 further illustrate this. Previous studies have suggested for this area crustal underplating during the ca. 1.08 Ga Warakurna LIP (Alghamdi et al., 2018) and contemporaneous mantle refertilisation (Aitken et al., 2023). This event is interpreted to explain the very thick crust here.

5.3. Magmatic-dominated rifting formed the thick crust of the Yilgarn Craton

In recent years, new geological and geochemical data have led to interpretations of the central Youanmi Terrane and Burtville Terrane to collectively represent a Mesoarchean proto-cratonic lithospheric block (Pawley et al., 2012), with the derivation of the EGST through Neo-archean rifting of this proto-craton (Masurel et al., 2022; Pawley et al., 2012; Schreefel et al., 2024; Smithies et al., 2024). A thinned lithosphere is expected beneath the rift axis, causing lithospheric mantle melting, and potentially entraining deeper-sourced magmatic upwellings into the rift. These para-autochtonous models of geological development contradict allochtonous interpretations that emphasized the accretion of exotic terranes to an older nucleus (Czarnota et al., 2010; Krapež and Barley, 2008; Standing, 2008). Notwithstanding the regions identified above, the exposed craton shows very limited tectonic reworking since 2.4 Ga, and its crustal structure should dominantly reflect Archean events.

For the exposed craton, Scenario 2 involves a moderate net extension with β-factor < 1.2, representing a maximum of 5 km of thinning of the proto-craton crust. The thicknesses of mafic magmatic addition to the crust are substantial; up to 14 km of magmatic addition in the EGST and up to 12 km in both the South West Terrane and the southern Youanmi Terrane. The interpretation is that rifting was magma-dominated, with the rate of magma input outpacing crustal extension to cause crustal thickening (Aitken et al., 2013b). Some caveats apply: if we consider not only extension but also later basin inversion and shortening, for example during the ca. 2.675–2.630 Ga Yilgarn Orogeny (Masurel and Thebaud., 2024) to reach today's crust, then this outcome would require increased extension and reduced magmatic addition; if the density of mafic material was increased, e.g. as garnet-bearing granulite with density 3134 kgm^{-3} (Rudnick and Fountain, 1995), this would reduce the need for extension slightly. Errors in the crustal density and crustal thickness will also generate slight differences in β-factor.

A key test for this scenario is to compare the magmatic addition to the crust against the isotopic signature of the craton's crustal evolution (Fig. 6). Although not directly indicative of volumetric juvenile input to the crust, we consider the predicted εHf at 2.600 Ga. εHf is predicted through co-kriging of data from recent compilations for Lu-Hf (Schreefel

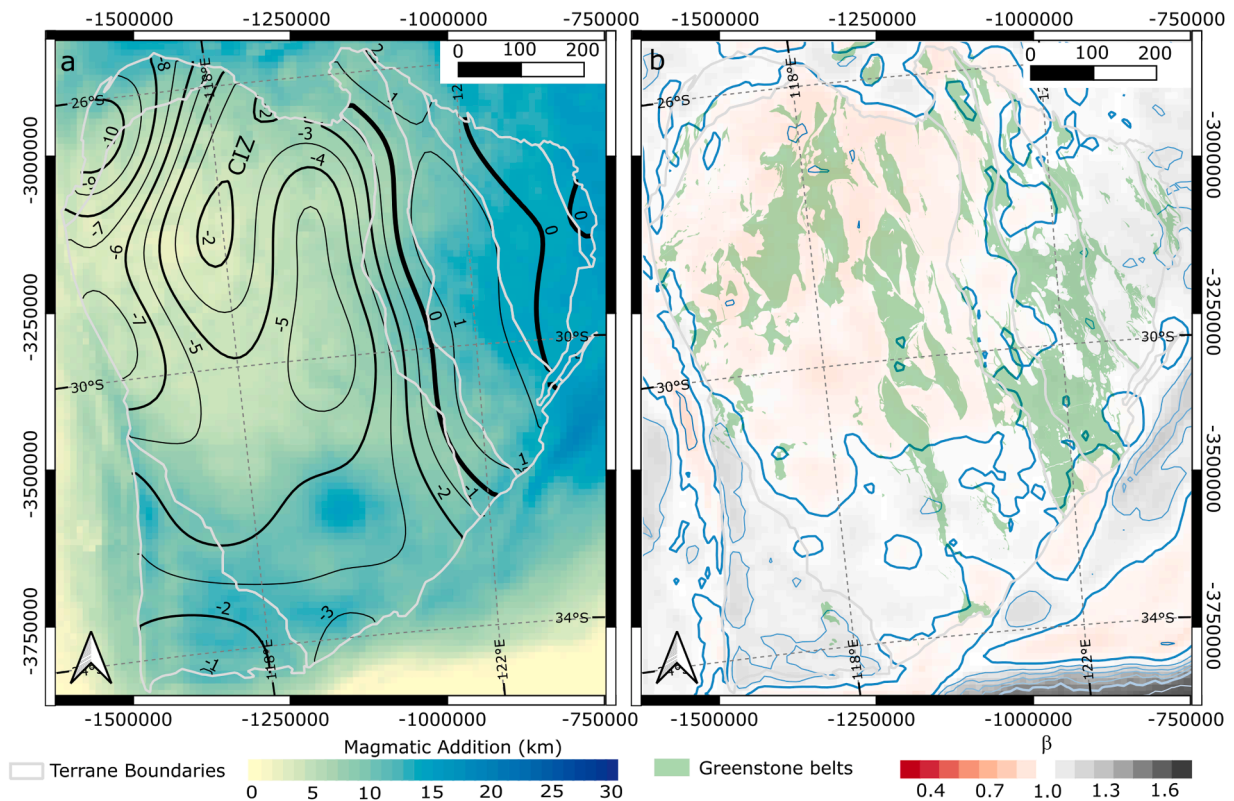**Fig. 6.** a) mafic magmatic addition from reconstruction scenario 2 with overlain contours of predicted εHf at 2.6 Ga from co-kriged Lu-Hf and Sm-Nd data (see supplement for details of kriging), b) β-factor from reconstruction scenario 2 with overlain greenstone belts. CIZ – Cue isotopic zone.

et al., 2024) and Sm-Nd (Lu et al., 2022). In the northern Youanmi Terrane, a broad zone with εHf < −4 corresponds to regions that have no known juvenile input after ca. 3.05 Ga (Mole et al., 2019). Inside this region, the Cue isotopic zone, which experienced extensive juvenile crust formation between ca. 2.82 Ga and 2.76 Ga (Smithies et al., 2024) has an εHf reaching −2. Neither has thickened crust nor net magmatic addition associated with crustal extension (Fig. 6). The southern isotopic zone of the Youanmi Terrane exhibits εHf between −4 and −2 (Fig. 6) that may highlight more substantial Neoarchean juvenile input than in its northern counterpart (Smithies et al., 2024). This region has notably thicker crust and magmatic input of 7–12 km.

The EGST with εHf > −1, experienced extensive juvenile crustal addition during the ca. 2.72 to 2.69 Ga Kalgoorlie Large Igneous Province, as defined in Hayman et al. (2015). The Kalgoorlie and Kurnalpi terranes are matched by substantial mafic and ultramafic magmatic addition to the mid-lower crust. The Kurnalpi Terrane, in particular, is associated with magmatic addition exceeding 10 km and εHf > 0 (Fig. 6b). The Burtville and Yamarna terranes present a hybrid Hf composition showing εHf ~ 0 and magmatic additions of >10 km. The South West Terrane has εHf > −4, reaching ~ −1 (Fig. 6a) suggesting moderate degrees of Neoarchean juvenile crust addition. There, thick crust and up to 12 km of magmatic addition is indicated.

The boundary between extended and unextended crust in scenario 2 defines, with some precision, the western limits of Neoarchean greenstone belts of the EGST (Fig. 6b). There is no similar relationship with Neoarchean greenstone belts in the South West Terrane or southern Youanmi Terrane, however, the evidence of juvenile crust formation in these regions is recorded in isotopic signatures of felsic igneous rocks (Smithies et al., 2024). Overall, except for the Cue isotopic zone, regions with less evolved crust at 2.600 Ga are associated with higher volumes of magmatic addition, suggesting that there is a positive relationship between juvenile crust formation in the Neoarchean and the formation of a thick and dense crust.

5.4. Stratigraphic, structural and metamorphic constraints on crustal development

Stratigraphic reconstructions across multiple greenstone belts in the Youanmi Terrane and EGST indicate ~130 Ma of magmatism between ca. 2.82 and 2.69 Ga with no significant hiatus (Austin et al 2022; Masurel et al., 2022). This magmatic continuum includes (i) ca. 2.82–2.74 Ga mafic–ultramafic volcanic rock successions, (ii) ca. 2.74–2.72 Ga felsic volcanic rocks, associated fragmental deposits and contemporaneous mafic–ultramafic intrusions, and (iii) ca. 2.72–2.69 Ga mafic–ultramafic volcanic rock successions and co-magmatic intrusions (Hayman et al., 2015; Masurel et al., 2022; Pawley et al., 2012; Witt et al., 2020). Within this stratigraphic scheme, pre-2.74 Ga deep-marine greenstones were uplifted, eroded, and unconformably overlain by ca. 2.74–2.72 Ga shallow-marine to subaerial clastic and felsic volcanic rock sequences (Zibra et al., 2017; Masurel et al., 2022).

The extent of this ca. 2.73 Ga stratigraphic unconformity remains poorly defined, but it is observed in the Youanmi, and Kalgoorlie terranes, inferred in the Kurnalpi Terrane, and can be viewed as a craton-wide feature, with the exception of the South West Terrane. Diverging views have attributed the unconformity to either (i) docking of the Narryer Terrane against the Youanmi Terrane (Masurel and Thébaud, 2024) or (ii) to deformation induced by the impingement of a mantle upwelling followed by the voluminous outpouring of primitive mafic-ultramafic volcanic products between 2.72–2.69 Ga (Masurel et al., 2022; Mole et al., 2019). The ca. 2.675–2.630 Ga Yilgarn Orogeny comprises a protracted sequence of deformation phases, marked by the activation of several shear zones through time and repeated shifts in the location of sedimentary depocenters (Czarnota et al., 2010; Masurel and Thébaud, 2024; Zibra, 2020).

Metamorphic grade across the craton is variable due to several overprinting metamorphic events, with a baseline at greenschist-facies punctuated by higher-grade metamorphism in high-strain regions, and other regions with sub-greenschist facies rocks preserved (Goscombe et al., 2019). In the EGST, metamorphic constraints indicate apparent near-isobaric (low-*P,* high-*T*) metamorphic conditions, with lateral temperature gradients related mainly to the emplacement of plutons (Goscombe et al., 2019). The tight clockwise P-T paths and low-P and high-T/depth ratios documented in the EGST between ca. 2.675 and 2.630 Ga (Goscombe et al., 2019), argue in favour of only moderate burial during crustal thickening (i.e. P_{max} = 6.5 kbar) associated with the Kalgoorlie Orogeny. The Youanmi Terrane shows variable metamorphic grade with generally similar grade to the EGST but with higher metamorphic grade locally (Goscombe et al., 2019). Amphibolite- and granulite-facies rocks are seen in the metamorphic belts aligned along the western edge of the craton, and in the Narryer Terrane (Goscombe et al., 2019). For these high-grade regions we may prefer scenario 1 with 10–15 km of differential erosion (Fig. 4a). The Corrigin Tectonic Zone also comprises granulite-facies gneisses but has neither high density nor thick crust (Fig. 3). This suggests sinistral transpression along the Corrigin Tectonic Zone between ca. 2.665 and 2.635 Ga (Quentin De Gromard et al., 2021) had a limited effect on bulk crustal thickness and density. At the scale of the craton, the laterally continuous stratigraphy coupled with the overall similarity in metamorphic grade (Goscombe et al., 2019) argue against scenario 1, whereby achieving the observed crustal density would require tens of kilometres of erosion and near-doubling of crustal thickness in the EGST relative to the Youanmi Terrane (Fig. 4). We conclude that while shortening is certainly an important modifier of crustal thickness and density, the dominant process of crustal thickening in the craton post ca. 2730 Ma was mafic magmatic addition as defined in scenario 2.

5.5. A step change in the Yilgarn Craton crust-forming process at ca. 2.73 ga

The tectonic evolution of the craton has recently been divided into pre-orogenic and syn-orogenic stages based on the identification of the ca. 2.73 Ga stratigraphic unconformity (Zibra et al., 2020, 2017). The only pre-orogenic structures recognized to date are associated with polydiapirism features (i.e. dome-and-keel architecture) in the core of the Yalgoo Dome in the Youanmi Terrane (Clos et al., 2019). In contrast, the 2.675–2.630 Ga Yilgarn Orogeny resulted in the development and activation of distinct shear zones under progressive ENE-WSW-directed bulk crustal shortening (Masurel and Thébaud, 2024; Zibra et al., 2020). The identification of a craton-wide ca. 2.73 Ga unconformity marks the first time when the surface emerged above sea level. Given a nearly continuous tectonic evolution, we argue that this event marks a major turning-point in the development of the lower-crust. The subsequent rifting event(s) in the EGST re-lowered the surface as well as thickening the crust through intense mantle-derived magmatic input over a time frame of ca. 40 Ma (Masurel et al., 2022).

Magmatic crustal thickening can occur through various processes, including the accumulation of magma at the base of the crust (underplating) and sill emplacement into the lower-middle crust (sill inflation). We do not have capacity from our model to directly constrain the mechanism. Seismic reflection surveys of the EGST resolve a reflective mid-crust grading to less reflective lower crust (Calvert and Doublier, 2018) suggesting intra-crustal sill inflation as a likely mechanism. In modern settings, magmatic crustal thickening can be driven by sill inflation with rates of opening for individual sills modelled between 20–40 mm/yr and with volumetric inputs of $2-4 \times 10^6$ m^3/yr (La Rosa et al., 2024). These volumes, averaged over the event area, yield a crustal magmatic addition rate of 3 mm/a over the short-term, i.e. years. If such rates are applied to our scenario 2, the crustal thickening may have involved up to ~5–7 Ma of active inflation occurring within the ~40 Ma period. Further work is needed to unravel the spatial and temporal distribution of mafic intrusive events across the craton, but a series of geographically and temporally discrete sill-inflation events is

suggested.

5.6. Just one step in time? the link to global evolution

The magmatic addition to the crust in scenario 2 represents a 5.0 Mkm^3 net addition. This event is regionally profound, but its impact on global average crustal thickness is clearly small. Here we consider how this event might fit into models of global crustal thickness evolution.

Some geochemical and isotopic data are linked empirically to crustal thickness and can provide a sample of local crustal thickness for a magmatic event, now or in the past (Luffi and Ducea, 2022). Several analyses have been applied seeking to understand crustal thickness evolution through time (Balica et al., 2020; Dhuime et al., 2015; Tang et al., 2021). From Eu/Eu* in zircon, Tang et al. (2021) identify a thickening Archean crust reaching 56 km at 3.0 Ga and a subsequent thinning in the Proterozoic reaching 41 km by 1.1 Ga. From (La/Yb)$_n$ in zircon, Balica et al. (2020) identify a jump in crustal thickness from 33 km to 38 km at ca. 3.2 Ga with the thick crust persisting to 1.9 Ga, and a decline to 30 km by 1.5 Ga. From Rb/Sr, Dhuime et al. (2015) modelled a crustal thickness increase from 15±13 km at 3.2 Ga to 40±5 km at 1.7 Ga. The mapping of Rb/Sr to SiO$_2$ is non-unique, with Rb/Sr variations able to be explained by varying intensity of mantle partial melting (Keller and Harrison, 2020).

Monte-Carlo simulations were run to fit the crustal thickness evolution models of Dhuime et al. (2015), Tang et al. (2021) and Balica et al. (2020). Data was trimmed to fit between 4.15 and 0.25 Ga to avoid edge effects. The simulations comprise numerous discrete crust addition/removal events, randomly distributed in time, with volumes of 0 ± 10 Mkm^3 and durations of 20 ± 20 Ma. Each event is a permanent addition or removal to crustal thickness. All model results are described in the supplement.

The simulation fitting to Dhuime et al. (2015) maps out several stages in global crustal evolution (Fig. 7). These involve variations in the frequency of destructive and constructive events with peaks in constructive tendency at 3.80, 2.75 and 2.10 Ga and peaks in destructive tendency at 3.40, 1.65, and 0.85 Ga. The Archean Yilgarn Craton crust evolution is in broad alignment with the global stages in this model: Early crustal elements were reworked to form the cratonic core by 3.30 Ga in stage 2A (Mole et al., 2019). Subsequently, major craton growth between 3.05 and 2.82 Ga formed a stable proto-craton in stage 2B (Mole et al., 2019). Crustal growth 2.73–2.69 Ga (Mole et al., 2019) formed in stage 2C, in line with a peak in constructive tendency (Fig. 7) after which the 2.675–2.630 Ga Yilgarn Orogeny is considered the main cratonisation event.

Our 5.0 MKm^3 event at 2.7 Ga is aligned with a peak in constructive tendency for both the Dhuime et al. (2015) and Balica et al. (2020) models. Our event is unaligned with Tang et al. (2021), who have a predominantly destructive tendency from 3.1 to 2.2 Ga, and only a local peak at 2.7 Ga. For all models, the deviations of central tendency are within the range ±4 Mkm^3 throughout, less than 1 standard deviation (σ = 5.77 Mkm^3), and none show a significant secular trend. These models indicate that the frequencies of constructive and destructive events have been broadly consistent since the Eoarchean, with moderate variations in central tendency sustained for periods of 400±200 Ma.

6. Conclusion

Seismic-constrained gravity inversions show that Yilgarn Craton partly fits the Archean paradigm of a relatively thin and low-density crust (Abbott et al., 2013), but has regions that possess a thicker and
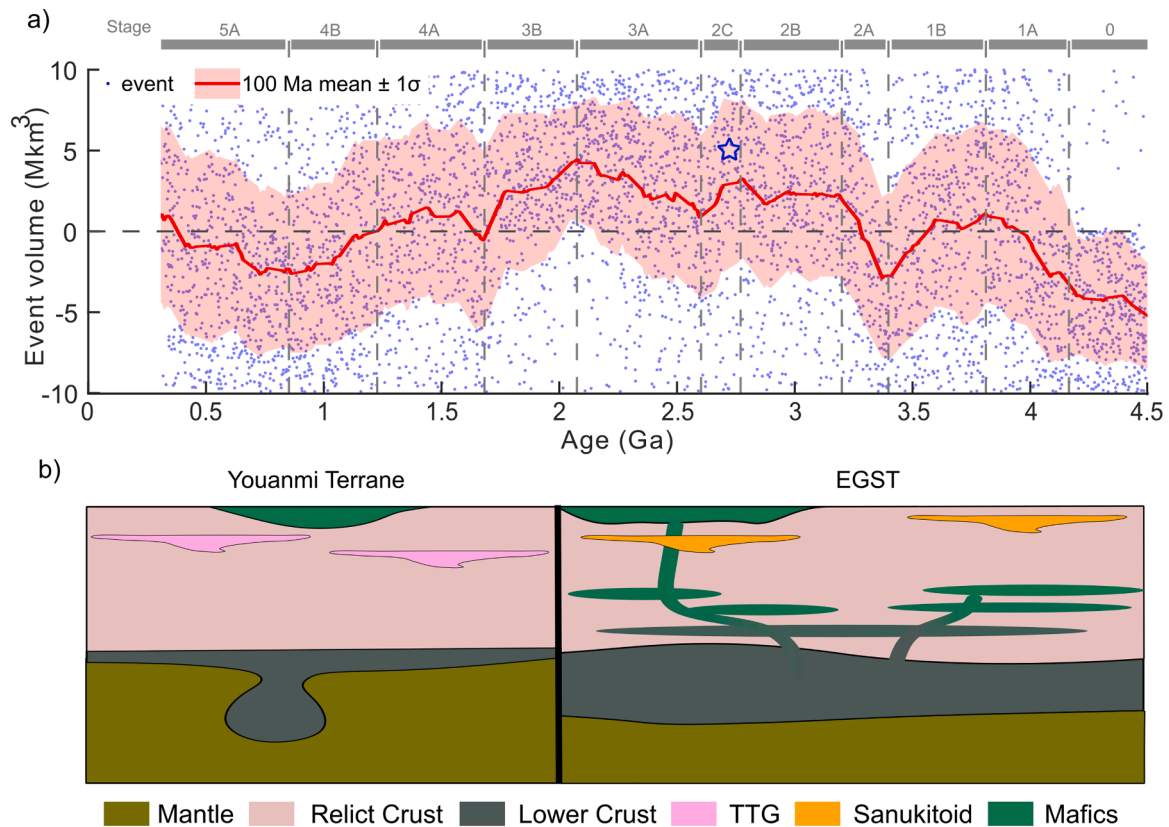

Fig. 7. a) Accepted events from the Monte-Carlo simulation for Dhuime et al. (2015). Each blue dot indicates an accepted event. The mean ± 1σ range for rolling 100 Ma windows is shown in red, while the blue star indicates the timing and magnitude of the 2.7 Ga event in the Yilgarn Craton. Details of the Monte Carlo simulation for this and the models of Tang et al. (2021) and Balica et al. (2020) are in the supplement. b) cartoon of the formation of the Youanmi Terrane crust and the subsequent formation of the EGST crust.

denser crust. Reconstruction of today's crust back to a reference crust representing the Mesoarchean Yilgarn proto-craton indicates that the crust was thickened by the addition of 5.0 MKm^3 of mafic magma, inferred to represent a distributed series of sill intrusions in the lower-middle crust. The modelled magmatic addition is greatest in regions that experienced juvenile crust formation in the period ca. 2.73 to 2.60 Ga, and least in regions that did not experience juvenile addition after ca. 2.80 Ga. A regional unconformity at ca. 2.73 Ga marks the time that the threshold for lower crust stability was reached in the Yilgarn Craton, enabling a thick and dense crust to form during subsequent rift events.

This example may be characteristic of at least one of the processes for the global transition of crustal structure. To test how this event sits within the global evolution, Monte-Carlo simulations were run for several crustal thickness evolution models. In two of the three models, the Yilgarn Craton event is identified in line with a global peak in constructive tendency at 2.7 Ga. For the Neoarchean crust transition, a diachronous development is suggested, as different regions reached geodynamic stability thresholds at different times. Further, these models showed that long-term variations in global average crustal thickness can be explained by moderate shifts in the central tendency towards constructive or destructive events that persist for periods of 200–600 Ma.

CRediT authorship contribution statement

Alan R.A. Aitken: Conceptualization, Data curation, Formal analysis, Funding acquisition, Investigation, Methodology, Project administration, Resources, Software, Visualization, Writing – original draft, Writing – review & editing. **Q. Masurel:** Conceptualization, Investigation, Writing – original draft, Writing – review & editing. **N. Thébaud:** Conceptualization, Funding acquisition, Investigation, Project administration, Supervision, Writing – original draft, Writing – review & editing. **Lu Li:** Data curation, Formal analysis, Investigation, Methodology, Software, Writing – original draft, Writing – review & editing, Writing – original draft. **Abdul Azim bin Rossalim:** Data curation, Formal analysis, Investigation, Methodology, Software, Writing – original draft, Writing – review & editing.

Declaration of competing interest

The authors declare that they have no known competing financial interests or personal relationships that could have appeared to influence the work reported in this paper.

Data and Code availability

All inputs to the work including crustal geometry information, gravity data and isotopic data are publicly available from the cited data sources. The VPmg inversion code is available on a commercial basis. Inversion model results and scripts for the reconstructions and Monte-Carlo simulation are available from Zenodo repository (10.5281/zenodo.12590616)

Supplementary materials

Supplementary material associated with this article can be found, in the online version, at doi:10.1016/j.epsl.2025.119336.

Data availability

All original research data and codes are available through Zenodo repository 10.5281/zenodo.12590616

References

Abbott, D.H., Mooney, W.D., Van Tongeren, J.A., 2013. The character of the Moho and lower crust within archean cratons and the tectonic implications. Tectonophysics 609, 690–705. https://doi.org/10.1016/J.TECTO.2013.09.014.

Aitken, A.R.A., Smithies, R.H., Dentith, M.C., Joly, A., Evans, S., Howard, H.M., 2013b. Magmatism-dominated intracontinental rifting in the Mesoproterozoic: the Ngaanyatjarra Rift, central Australia. Gondwana Res. 24. https://doi.org/10.1016/j.gr.2012.10.003.

Aitken, A.R.A., Fiorentini, M., Tesauro, M., Thébaud, N., 2023. Supercontinent-paced magmatic destabilisation and recratonisation of the Yilgarn Craton. Gondwana Res. 116, 12–24. https://doi.org/10.1016/j.gr.2022.11.016.

Aitken, A.R.A., 2010. Moho geometry gravity inversion experiment (MoGGIE): a refined model of the Australian Moho, and its tectonic and isostatic implications. Earth Planet Sci. Lett. 297. https://doi.org/10.1016/j.epsl.2010.06.004.

Aitken, A.R.A., Salmon, M.L., Kennett, B.L.N., 2013a. Australia's Moho: a test of the usefulness of gravity modelling for the determination of Moho depth. Tectonophysics 609. https://doi.org/10.1016/j.tecto.2012.06.049.

Alghamdi, A.H., Aitken, A.R.A., Dentith, M.C., 2018. The deep crustal structure of the Warakurna LIP, and insights on proterozoic LIP processes and mineralisation. Gondwana Res. 56, 1–11. https://doi.org/10.1016/j.gr.2017.12.001.

J.M. Austin, P.C. Hayman, D.T. Murphy, M.T.D. Wingate, Y. Lu, J. Lowrey, K. Rose, The voluminous 2.81–2.71 Ga Goldfields Tholeiitic Super Event: Implications for basin architecture in the Yilgarn Craton and global correlations, Precambrian Research, Volume 369, 2022, 106528, ISSN 0301-9268 https://doi.org/10.1016/j.precamres.2021.106528.

Balica, C., Ducea, M.N., Gehrels, G.E., Kirk, J., Roban, R.D., Luffi, P., Chapman, J.B., Triantafyllou, A., Guo, J., Stoica, A.M., Ruiz, J., Balintoni, I., Profeta, L., Hoffman, D., Petrescu, L., 2020. A zircon petrochronologic view on granitoids and continental evolution. Earth Planet Sci. Lett. 531. https://doi.org/10.1016/J.EPSL.2019.116005.

Brenhin Keller, C., Schoene, B., 2012. Statistical geochemistry reveals disruption in secular lithospheric evolution about 2.5 gyr ago. Nature 485, 490–493. https://doi.org/10.1038/nature11024, 20127399 485.

Calvert, A.J., Doublier, M.P., 2018. Archaean continental spreading inferred from seismic images of the Yilgarn Craton. Nat. Geosci. 11, 526–530. https://doi.org/10.1038/s41561-018-0138-0.

Clos, F., Weinberg, R.F., Zibra, I., Schwindinger, M., 2019. Magmatic and anatectic history of a large Archean diapir: insights from the migmatitic core of the Yalgoo Dome, Yilgarn Craton. Lithos 18–33. https://doi.org/10.1016/J.LITHOS.2019.04.012, 338–339.

Czarnota, K., Champion, D.C., Goscombe, B., Blewett, R.S., Cassidy, K.F., Henson, P.A., Groenewald, P.B., 2010. Geodynamics of the eastern Yilgarn Craton. Precambrian Res. 183, 175–202. https://doi.org/10.1016/j.precamres.2010.08.004.

de Vries, S.T., Pryer, L.L., Fry, N., 2008. Evolution of neoarchaean and proterozoic basins of Australia. Precambrian Res. 166, 39–53. https://doi.org/10.1016/J.PRECAMRES.2008.01.005.

Dhuime, B., Wuestefeld, A., Hawkesworth, C.J., 2015. Emergence of modern continental crust about 3 billion years ago. Nat. Geosci. 8, 552–555. https://doi.org/10.1038/ngeo2466.

Foerste, C., Bruinsma, Sean.L., Abrykosov, O., Lemoine, J.-M., Marty, J.C., Flechtner, F., Balmino, G., Barthelmes, F., Biancale, R., 2014. EIGEN-6C4 The latest Combined Global Gravity Field Model Including GOCE Data Up to Degree and Order 2190 of GFZ Potsdam and GRGS Toulouse. GFZ Data Services.

Ganne, J., Feng, X., 2017. Primary magmas and mantle temperatures through time. Geochem. Geophys. Geosyst. 18, 872–888. https://doi.org/10.1002/2016GC006787.

Geognostics Australia Pty Ltd, 2021. OZ SEEBASE® 2021 (Version 1, May 2021). https://www.geognostics.com/oz-seebase-2021 [WWWDocument].

Glasson, K.J., Johnson, T.E., Kirkland, C.L., Gardiner, N.J., Clark, C., Blereau, E., Hartnady, M.I.H., Spaggiari, C., Smithies, H., 2019. A Window Into an Ancient backarc? The magmatic and Metamorphic History of the Fraser Zone, 323. Precambrian Res, Western Australia, pp. 55–69. https://doi.org/10.1016/j.precamres.2019.01.011.

Goscombe, B., Foster, D.A., Blewett, R., Czarnota, K., Wade, B., Groenewald, B., Gray, D., 2019. Neoarchaean metamorphic evolution of the Yilgarn Craton: a record of subduction, accretion, extension and lithospheric delamination. Precambrian Res. 335. https://doi.org/10.1016/j.precamres.2019.105441.

Hawkesworth, C.J., Cawood, P.A., Dhuime, B., 2020. The evolution of the continental crust and the onset of plate tectonics. Front Earth Sci. 8. https://doi.org/10.3389/feart.2020.00326.

Hayman, P.C., Thébaud, N., Pawley, M.J., Barnes, S.J., Cas, R.A.F., Amelin, Y., Sapkota, J., Squire, R.J., Campbell, I.H., Pegg, I., 2015. Evolution of a ~2.7Ga large igneous province: a volcanological, geochemical and geochronological study of the Agnew Greenstone Belt, and new regional correlations for the Kalgoorlie Terrane (Yilgarn Craton, Western Australia). Precambrian Res. 270, 334–368. https://doi.org/10.1016/j.precamres.2015.09.016.

Herzberg, C., Condie, K., Korenaga, J., 2010. Thermal history of the Earth and its petrological expression. Earth Planet Sci. Lett. 292, 79–88. https://doi.org/10.1016/j.epsl.2010.01.022.

Johnson, T.E., Brown, M., Kaus, B.J.P., Van Tongeren, J.A., 2014. Delamination and recycling of Archaean crust caused by gravitational instabilities. Nat. Geosci. 7, 47–52. https://doi.org/10.1038/ngeo2019.

Keller, C.B., Harrison, T.M., 2020. Constraining crustal silica on ancient Earth. Proc. Natl. Acad. Sci. U S A 117, 21101–21107. https://doi.org/10.1073/pnas.2009431117.

Kennett, B.L.N., Fichtner, A., Fishwick, S., Yoshizawa, K., 2013. Australian seismological referencemodel (AuSREM): mantle component. Geophys. J. Int. 192. https://doi.org/10.1093/gji/ggs065.

Kennett, B.L.N., Gorbatov, A., Yuan, H., Agrawal, S., Murdie, R., Doublier, M.P., Eakin, C. M., Miller, M.S., Zhao, L., Czarnota, K., Dentith, M., Gessner, K., 2023. Refining the Moho across the Australian continent. Geophys. J. Int. 233, 1863–1877. https://doi.org/10.1093/gji/ggad035.

Korenaga, J., 2018. Crustal evolution and mantle dynamics through Earth history. Philosop. Trans. Royal Society A: Math. Phys. Eng. Sci. 376. https://doi.org/10.1098/RSTA.2017.0408.

Korsch, R.J., Doublier, M.P., 2016. Major crustal boundaries of Australia, and their significance in mineral systems targeting. Ore. Geol. Rev. 76, 211–228. https://doi.org/10.1016/J.OREGEOREV.2015.05.010.

Krapež, B., Barley, M.E., 2008. Late archaean synorogenic basins of the Eastern Goldfields Superterrane, Yilgarn Craton, Western Australia: part III. Signatures of tectonic escape in an arc-continent collision zone. Precambrian Res. 161, 183–199. https://doi.org/10.1016/J.PRECAMRES.2007.06.020.

La Rosa, A., Pagli, C., Wang, H., Sigmundsson, F., Pinel, V., Keir, D., 2024. Simultaneous rift-scale inflation of a deep crustal sill network in Afar, East Africa. Nat. Commun. 15, 4287. https://doi.org/10.1038/s41467-024-47136-4.

Lane, R.J.L., Wynne, P.E., Poudjom Djomani, Y., Stratford, W.R., Barretto, J.A., Caratori Tontini, F., 2020. 2019 Australian National Gravity Grids: Free Air Anomaly, Complete Bouguer Anomaly, De-trended Global Isostatic Residual, 400 m Cell Size (includes Point Located Data). Geoscience Australia, Canberra. https://pid.geoscience.gov.au/dataset/ga/133023.

Li, L., Aitken, A.R.A., 2024. Crustal heterogeneity of Antarctica signals spatially variable radiogenic heat production. Geophys. Res. Lett. 51. https://doi.org/10.1029/2023GL106201 e2023GL106201.

Lu, Y.-J., Wingate, M.T.D., Champion, D., Smithies, R.H., Johnson, S.P., Gessner, K., Maas, R., Mole, D.R., Poujol, M., Zhao, J.-X., Creaser, R.A., 2022. Samarium-neodymium isotope map of Western Australia 8 p.

Luffi, P., Ducea, M.N., 2022. Chemical mohometry: assessing crustal thickness of ancient orogens using geochemical and isotopic data. Rev. Geophys. 60. https://doi.org/10.1029/2021RG000753 e2021RG000753.

Mai, V.V., Korenaga, J., 2022. What controlled the thickness of continental crust in the Archean? Geology 50, 1091–1095. https://doi.org/10.1130/G50350.1.

Markwitz, V., Kirkland, C.L., Wyrwoll, K.H., Hancock, E.A., Evans, N.J., Lu, Y., 2017. Variations in Zircon provenance constrain age and geometry of an early paleozoic rift in the Pinjarra Orogen, East Gondwana. Tectonics 36, 2477–2496. https://doi.org/10.1002/2017TC004696.

Masurel, Q., Thébaud, N., 2024. Deformation in the Agnew-Wiluna Greenstone Belt and host Kalgoorlie Terrane during the c. 2675–2630 ma Kalgoorlie Orogeny: 45 ma of horizontal shortening in a neoarchean back-arc region. Precambrian Res. 414, 107586. https://doi.org/10.1016/J.PRECAMRES.2024.107586.

Masurel, Q., Thébaud, N., Sapkota, J., De Paoli, M.C., Drummond, M., Smithies, R.H., 2022. Stratigraphy of the Agnew-Wiluna Greenstone Belt: review, synopsis and implications for the late mesoarchean to neoarchean geological evolution of the Yilgarn Craton. Australian J. Earth Sci. 69, 1149–1176. https://doi.org/10.1080/08120099.2022.2102076.

Mole, D.R., Kirkland, C.L., Fiorentini, M.L., Barnes, S.J., Cassidy, K.F., Isaac, C., Belousova, E.A., Hartnady, M., Thebaud, N., 2019. Time-space evolution of an archean craton: a Hf-isotope window into continent formation. Earth Sci. Rev. 196. https://doi.org/10.1016/j.earscirev.2019.04.003.

Mooney, W.D., Barrera-Lopez, C., Suárez, M.G., Castelblanco, M.A., 2023. Earth crustal Model 1 (ECM1): a 1° x 1° global seismic and density model. Earth Sci. Rev. 243, 104493. https://doi.org/10.1016/J.EARSCIREV.2023.104493.

Moro, P.S., Aitken, A.R.A., Giraud, J., Jessell, M.W., Kohan Pour, F., 2023. Seismically constrained gravity inversions reveal magmatic and metamorphic processes at a major lithospheric boundary in northwestern Australia. Tectonophysics 863. https://doi.org/10.1016/j.tecto.2023.230003.

Moyen, J.-F., Martin, H., 2012. Forty years of TTG research. Lithos 148, 312–336. https://doi.org/10.1016/J.LITHOS.2012.06.010.

Oakey, G.N., Saltus, R.W., 2016. Geophysical analysis of the Alpha–Mendeleev ridge complex: characterization of the high Arctic large igneous province. Tectonophysics 691, 65–84. https://doi.org/10.1016/J.TECTO.2016.08.005.

Occhipinti, S., Hocking, R., Lindsay, M., Aitken, A., Copp, I., Jones, J., Sheppard, S., Pirajno, F., Metelka, V., 2017. Paleoproterozoic Basin Development On the Northern Yilgarn Craton, 300. Precambrian Res, Western Australia, pp. 121–140. https://doi.org/10.1016/j.precamres.2017.08.003.

Pawley, M.J., Wingate, M.T.D., Kirkland, C.L., Wyche, S., Hall, C.E., Romano, S.S., Doublier, M.P., 2012. Adding pieces to the puzzle: episodic crustal growth and a new terrane in the northeast Yilgarn Craton, Western Australia. Australian J. Earth Sci. 59, 603–623. https://doi.org/10.1080/08120099.2012.696555.

Qashqai, M.T., Saygin, E., 2019. Moho structure of Australia from probabilistic inversion of teleseismic P-wave coda autocorrelation. Explorat. Geophys. https://doi.org/10.1080/22020586.2019.12073108, 2019.

Quentin De Gromard, R., Ivanic, T.J., Zibra, I., 2021. Pre-mesozoic interpreted bedrock geology of the southwest Yilgarn, 2021. Geological Survey of Western Australia. Digital Data Layer.

Ramos, L.N., Aitken, A.R.A., Occhipinti, S.M., Lindsay, M.D., 2021. Rift structures and magmatism focus VMS and gold mineralisation in the paleoproterozoic Bryah Rift Basin. Australia. Ore. Geol. Rev. 135. https://doi.org/10.1016/j.oregeorev.2021.104192.

Reading, A.M., Kennett, B.L.N., Goleby, B., 2007. New constraints on the seismic structure of West Australia: evidence for terrane stabilization prior to the assembly of an ancient continent? Geology 35, 379–382. https://doi.org/10.1130/G23341A.1.

Rudnick, R.L., Fountain, D.M., 1995. Nature and composition of the continental crust: a lower crustal perspective. Rev. Geophys. 33, 267–309. https://doi.org/10.1029/95RG01302.

Schreefel, R., Fisher, C.M., Kemp, I.S., A, Hagemann, S.G., Masurel, Q., Thébaud, N., Davy's, C., A, J., Martin, L., Lowrey, J.R., Lu, Y., Cassidy, K.F., 2024. Crustal Growth in the Archean: Insights from Zircon Petrochronology of the Far-East Yilgarn Craton, 401. Precambrian Res, Western Australia, 107253. https://doi.org/10.1016/J.PRECAMRES.2023.107253.

Sellars, S.E., Calvert, A.J., Doublier, M.P., 2022. Seismic reflection and potential field constraints on imbrication and exhumation of the paleoarchean Narryer Terrane, Yilgarn Craton. Tectonics 41. https://doi.org/10.1029/2022TC007343.

Smithies, R.H., Gessner, K., Lu, Y., Kirkland, C.L., Ivanic, T., Lowrey, J.R., Champion, D. C., Sapkota, J., Masurel, Q., Thébaud, N., de Gromard, R.Q., 2024. Geochemical mapping of lithospheric architecture disproves Archean terrane accretion in the Yilgarn craton. Geology 52, 141–146. https://doi.org/10.1130/G51707.1.

Spaggiari, C.V., Kirkland, C.L., Smithies, R.H., Wingate, M.T.D., Belousova, E.A., 2015. Transformation of an Archean craton Margin During Proterozoic basin Formation and magmatism: The Albany-Fraser Orogen, 266. Precambrian Res, Western Australia, pp. 440–466. https://doi.org/10.1016/j.precamres.2015.05.036.

Standing, J.G., 2008. Terrane amalgamation in the Eastern Goldfields Superterrane, Yilgarn Craton: evidence from tectonostratigraphic studies of the Laverton Greenstone Belt. Precambrian Res. 161, 114–134. https://doi.org/10.1016/j.precamres.2007.06.015.

Szwillus, W., Afonso, J.C., Ebbing, J., Mooney, W.D., 2019. Global crustal thickness and velocity structure from geostatistical analysis of seismic data. J. Geophys. Res. Solid Earth 124, 1626–1652. https://doi.org/10.1029/2018JB016593.

Tang, M., Lee, C.-T.A., Rudnick, R.L., Condie, K.C., 2020. Rapid mantle convection drove massive crustal thickening in the late Archean. Geochim. Cosmochim. Acta 278, 6–15. https://doi.org/10.1016/j.gca.2019.03.039.

Tang, M., Chu, X., Hao, J., Shen, B., 2021. Orogenic quiescence in Earth's middle age. Science 371, 728–731. https://doi.org/10.1126/science.abf1876, 1979.

Tesauro, M., Kaban, M.K., Aitken, A.R.A., 2020. Thermal and compositional anomalies of the australian upper mantle from seismic and gravity data. Geochem. Geophys. Geosyst. 21. https://doi.org/10.1029/2020GC009305.

Tucker, N.M., Hammerli, J., Kemp, A.I.S., Rowe, M.L., Gray, C.M., Jeon, H., Whitehouse, M.J., Roberts, M.P., 2024. Ultrahigh thermal gradient granulites in the Narryer Terrane, Yilgarn Craton, Western Australia, provide a window into the composition and formation of archean lower crust. J. Metamorphic Geo. 42, 425–470. https://doi.org/10.1111/jmg.12752.

Whiteway, T., 2009. Australian Bathymetry and Topography Grid, June 2009. Canberra.

Witt, W.K., Cassidy, K.F., Lu, Y.-J., Hagemann, S.G., 2020. The tectonic setting and evolution of the 2.7 Ga Kalgoorlie–Kurnalpi Rift, a world-class archean gold province. Miner Depos. 55, 601–631. https://doi.org/10.1007/s00126-017-0778-9.

Yuan, H., 2015. Secular change in Archean crust formation recorded in Western Australia. Nat. Geosci. 8, 808–813. https://doi.org/10.1038/ngeo2521.

Zibra, I., Clos, F., Weinberg, R.F., Peternell, M., 2017. The ~2730 ma onset of the neoarchean Yilgarn Orogeny. Tectonics 36, 1787–1813. https://doi.org/10.1002/2017TC004562.

Zibra, I., Lu, Y., Clos, F., Weinberg, R.F., Peternell, M., Wingate, M.T.D., Prause, M., Schiller, M., Tilhac, R., 2020. Regional-scale polydiapirism predating the Neoarchean Yilgarn Orogeny. Tectonophysics 779. https://doi.org/10.1016/j.tecto.2020.228375.